Molecular Microbiology (2011) 82(6), 1316–1329 ■
doi:10.1111/j.1365-2958.2011.07874.x
First published online 23 November 2011

Magnetosome chains are recruited to cellular division sites and split by asymmetric septation

Emanuel Katzmann,[1,2] Frank D. Müller,[1] Claus Lang,[1†] Maxim Messerer,[1] Michael Winklhofer,[3] Jürgen M. Plitzko[2] and Dirk Schüler[1*]
[1]*Ludwig-Maximilians-Universität München, Department Biology I, Biozentrum, D-82152 Planegg-Martinsried, Germany.*
[2]*Max Planck Institute of Biochemistry, Department of Molecular Structural Biology, D-82152 Planegg-Martinsried, Germany.*
[3]*Ludwig-Maximilians-Universität München, Department of Earth and Environmental Sciences, D-80333 Munich, Germany.*

Summary

Magnetotactic bacteria navigate along magnetic field lines using well-ordered chains of membrane-enclosed magnetic crystals, referred to as magnetosomes, which have emerged as model to investigate organelle biogenesis in prokaryotic systems. To become divided and segregated faithfully during cytokinesis, the magnetosome chain has to be properly positioned, cleaved and separated against intrachain magnetostatic forces. Here we demonstrate that magnetotactic bacteria use dedicated mechanisms to control the position and division of the magnetosome chain, thus maintaining magnetic orientation throughout divisional cycle. Using electron and time-lapse microscopy of synchronized cells of *Magnetospirillum gryphiswaldense*, we confirm that magnetosome chains undergo a dynamic pole-to-midcell translocation during cytokinesis. Nascent chains were recruited to division sites also in division-inhibited cells, but not in a *mamK* mutant, indicating an active mechanism depending upon the actin-like cytoskeletal magnetosome filament. Cryo-electron tomography revealed that both the magnetosome chain and the magnetosome filament are spilt into halves by asymmetric septation and unidirectional indentation, which we interpret in terms of a specific adaptation required to overcome the magnetostatic interactions between separating daughter chains. Our study demonstrates that magnetosome division and segregation is co-ordinated with cytokinesis and resembles partitioning mechanisms of other organelles and macromolecular complexes in bacteria.

Accepted 5 October, 2011. *For correspondence. E-mail dirk.schueler@lrz.uni-muenchen.de; Tel. (+49) 89218074502; Fax (+49) 89218074515. †Present address: Department of Biology, Stanford University, Stanford, CA 94305, USA.

Introduction

Magnetosomes are unique intracellular organelles used by magnetotactic bacteria to navigate along the Earth's magnetic field towards growth-favouring microoxic zones in their aquatic habitats (Jogler and Schüler, 2009). In *Magnetospirillum gryphiswaldense* MSR-1 (in the following referred to as MSR) and related magnetotactic bacteria, magnetosomes are membrane-enveloped sub-100 nm crystals of magnetite (Fe_3O_4) that are aligned in well-ordered chains (Jogler and Schüler, 2009; Murat *et al.*, 2010). Because of their complexity and resemblance to eukaryotic intracellular organelles, magnetosomes have recently emerged as model to investigate organelle biogenesis in prokaryotic systems (Faivre and Schüler, 2008; Murat *et al.*, 2010). Formation of functional magnetosome chains includes (i) the invagination of magnetosome membrane vesicles from the cytoplasmic membrane (Komeili *et al.*, 2006; Katzmann *et al.*, 2010) (ii) transport of iron into the magnetosome membrane vesicles and crystallization of magnetite (Faivre *et al.*, 2007; 2010), and (iii) assembly of crystals into a coherent linear chain along a dedicated cytoskeletal structure, the magnetosome filament (Frankel and Bazylinski, 2006; Komeili *et al.*, 2006; Scheffel *et al.*, 2006; Faivre *et al.*, 2010). It has been shown by a number of recent studies that each step is genetically controlled to achieve one of the highest structural levels found in a bacterial cell (Jogler and Schüler, 2009; Murat *et al.*, 2010).

During cytokinesis, bacterial cells have to duplicate and segregate their cellular content, such as plasmids and chromosomes (Gerdes *et al.*, 2010; Salje *et al.*, 2010). Magnetotactic bacteria face the additional challenge of dividing and equipartitioning the magnetosome chain preferably to pass on the selective advantage of magnetotaxis to both daughter cells. To ensure proper distribution and equal inheritance of functional magnetosome chains during cytokinesis, the magnetosome chain has to be positioned at the cellular division site, where it will be

split and separated against the cohesive forces caused by magnetostatic interactions between nascent daughter chains. However, it has remained unresolved how this is accomplished and co-ordinated with bacterial cell division.

Several recent observations suggested that magnetosome chain segregation may not occur randomly, but is subject to genetic control. Deletions of two genes were found to affect the assembly and positioning of the magnetosome chain in MSR: Loss of the actin-like MamK protein, which forms the cytoskeletal magnetosome filament, resulted in shorter, fragmented and ectopic (i.e. off-centre) chains (Katzmann *et al*., 2010), whereas loss of MamJ that is thought to connect magnetosome particles to the magnetosome filament, led to agglomerate magnetosome clusters (Scheffel *et al*., 2006), which were frequently mispartitioned to daughter cells by 'all-or-nothing' distribution (Scheffel and Schüler, 2007). This implied that the MamK filament might have a crucial role in concatenating and intracellular positioning of the magnetosome chain rather than just providing a rigid scaffold (Katzmann *et al*., 2010). In addition, it was noted that magnetosomes undergo dynamic localization during chain assembly (Scheffel and Schüler, 2007; Katzmann *et al*., 2010). Recently, it was suggested that chain structures may perform a sudden 'jump' in position upon completion of cell division (Staniland *et al*., 2010). In this study, Staniland and colleagues investigated the position of magnetosome chains throughout cell division of MSR by transmission electron microscopy, and based on the low abundance of cells with off-centered chains they concluded that the magnetosome chain may be dynamic and could move rapidly back to the centre of the cell after being cleaved.

Here we provide further evidence that magnetotactic bacteria use dedicated mechanisms for proper positioning and division of the magnetosome chain, rendering both daughter cells capable of magnetic orientation throughout the cell cycle. We demonstrate that magnetosome chain division is spatially and temporally co-ordinated with cytokinesis by recruitment and translocation of nascent chains to cellular division sites, which is followed by splitting of both the magnetosome chain and filament by asymmetric septation and unidirectional indentation. We hypothesize that this unique mechanism of asymmetric cell division and magnetosome chain cleavage represents a specific adaptation, which is required to overcome the substantial cohesive magnetostatic forces within the magnetosome chain during division of cells.

Results

Electron and time-lapse microscopy of the MSR cell cycle

Based on morphological features such as length-to-width ratios and degrees of constriction, electron micrographs of more than 50 representative cells from synchronized cultures were placed in relative order approximating the progression through cell division. This suggested a sequence of distinct events comprising (i) elongation of cells, (ii) constriction approximately at midcell, (iii) unidirectional bending and (iv) separation of newborn cells. In predivisional wild-type (WT) cells, magnetosome chains were consistently located at midcell, so that the chain became bent and eventually split into two daughter chains of approximately equal particle numbers that segregated evenly to daughter cells (Fig. 1A), similar as described previously (Sato *et al*., 1995; Yang *et al*., 2001; Staniland *et al*., 2010). Notably, at advanced stages of constriction, the proportion of cells with two-stranded chains traversing the division site was increased (Fig. S1). In contrast, Δ*mamK* cells had multiple, fragmented and shorter chains that were located randomly along the entire length of the cell at all stages. Even at late division chains often could be found close to cell poles, resulting in uneven segregation of magnetosome crystals (Fig. 1Bvi).

We also investigated dynamics and timing of division in living cells by time-lapse differential interference contrast (DIC) microscopy. While many cells (> 30) ceased growth and underwent spontaneous lysis during observation, in some cells (>10) the entire cycle could be followed for up to three generations. At first, extensive elongation occurred for about 120–180 min with a nearly linear length increase of about 5.4 nm per min (Fig. 2A and B) to reach a final length of about 5 μm. Elongation was followed by a second phase lasting another 40 min, in which cells gradually constricted at midcell. Similar as observed in previous studies in MSR (Staniland *et al*., 2010) and *M. magneticum* (Yang *et al*., 2001), this was accompanied by bending around the constriction point up to an angle of about 50°, which eventually resulted in fast separation ('snapping') of the two daughter cells. Acute bending and snapping proceeded very fast in less than 7 min (i.e. the time between two exposures). The entire cell cycle was completed after ~260 min, with a variability of < 30 min between different dividing cells (Figs 1C and 2B, Movie S1). This doubling time is shorter than in previous studies in which doubling times were estimated by averaging one bulk population including unknown proportions of dead and slowly growing cells. In cells dividing for multiple generations, speed of growth and final cell length gradually decreased to 280 min for completion of a full cycle and a maximum length of the mother cells of 4.5 μm during microscopic examination (Fig. 2B). Curiously, most cells elongated asymmetrically, as one of the two poles moved faster and further relative to extracellular reference points close to the cell centre (Fig. 2C–E, Movie S3). This resulted in pairs of daughter cells with lengths differing by 15% on average (maximum difference 60%), which

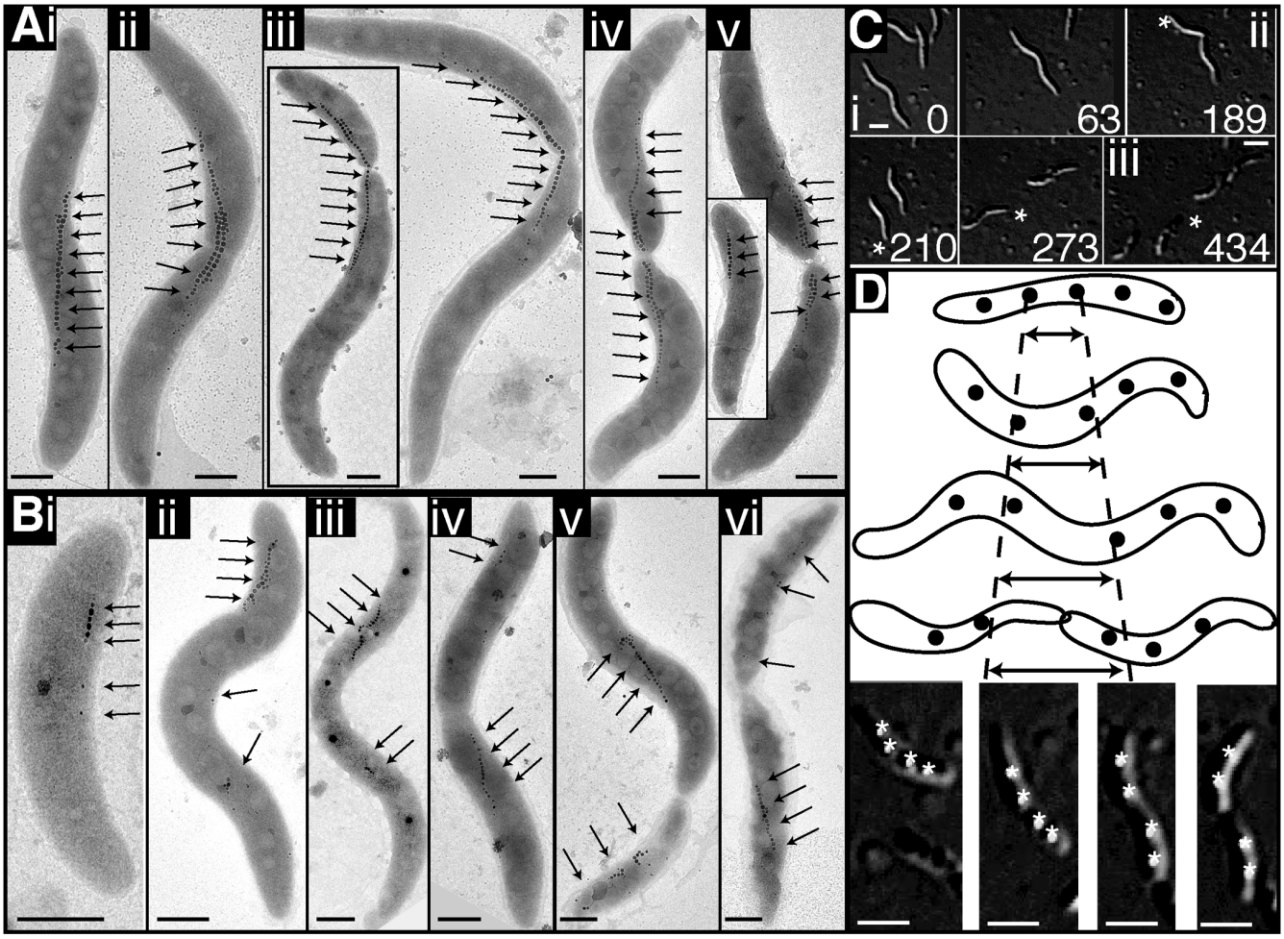

Fig. 1. TEM micrographs of individual WT (A) and Δ*mamK* (B) cells arranged by progression through division cycle (i–v/vi). Inset Av: Cell with sub-polar magnetosome chain. Scale bar 500 nm. Arrows indicate positions of magnetosome crystals.
C. Selected frames of DIC time-lapse series showing two offspring generations of a dividing WT cell (Movie S1). Scale bar 1 μm. Intervals of exposures are indicated in minutes; i–iii: number of generations; asterisks indicate positions of the same cell.
D. Schematic representation (upper panel) of intracellular PHB localization in dividing cells analysed by DIC microscopy (lower panel, Movie S2). Asterisk: positions of PHB granules. Scale bar 1 μm.

was also apparent from the analysis of several electron micrographs (e.g. inset Fig. 1Aiii and Bv).

In electron micrographs, strictly polar localization of magnetosome chains was only rarely observed in fully separated WT cells (inset Fig. 1Av), again suggesting a fast translocation of chains to midcell after division. This could be explained by either (i) fast cell growth at the new pole, or (ii) intracellular movement of magnetosome chains away from the new pole as suggested recently (Staniland *et al*., 2010). To identify zones of active cellular growth, we tracked the relative movement of intracellular polyhydroxybutyrate (PHB) granules in elongating cells. While PHB granules became rapidly separated at midcell, intergranular spacing remained invariant in polar regions (Fig. 1D and Movie S2). Assuming a transiently fixed position of granules relative to the adjacent cell wall (Williams, 1959), this argues against a polar mode of growth, but is consistent with elongation of the central sidewalls, much like in most rod-shaped bacteria having MreB (Margolin, 2009).

Recruitment of magnetosome chains to future division sites is mediated by MamK

As the previous observations implied an active magnetosome chain translocation from new poles to midcell during cytokinesis, we asked if chain localization is governed by spatial information provided by division sites in division-inhibited cells. The β-lactam antibiotic cephalexin inhibits the septum-specific penicillin-binding-protein 3 (FtsI). This allows major parts of the divisome to assemble, whereas final septation and cell separation are blocked (Pogliano *et al*., 1997). Treatment of MSR with 10 μg ml^{-1} cephalexin reversibly caused highly elongated (up to 62 μm) cells that still were magnetotactic as indicated by slow swimming and magnetic

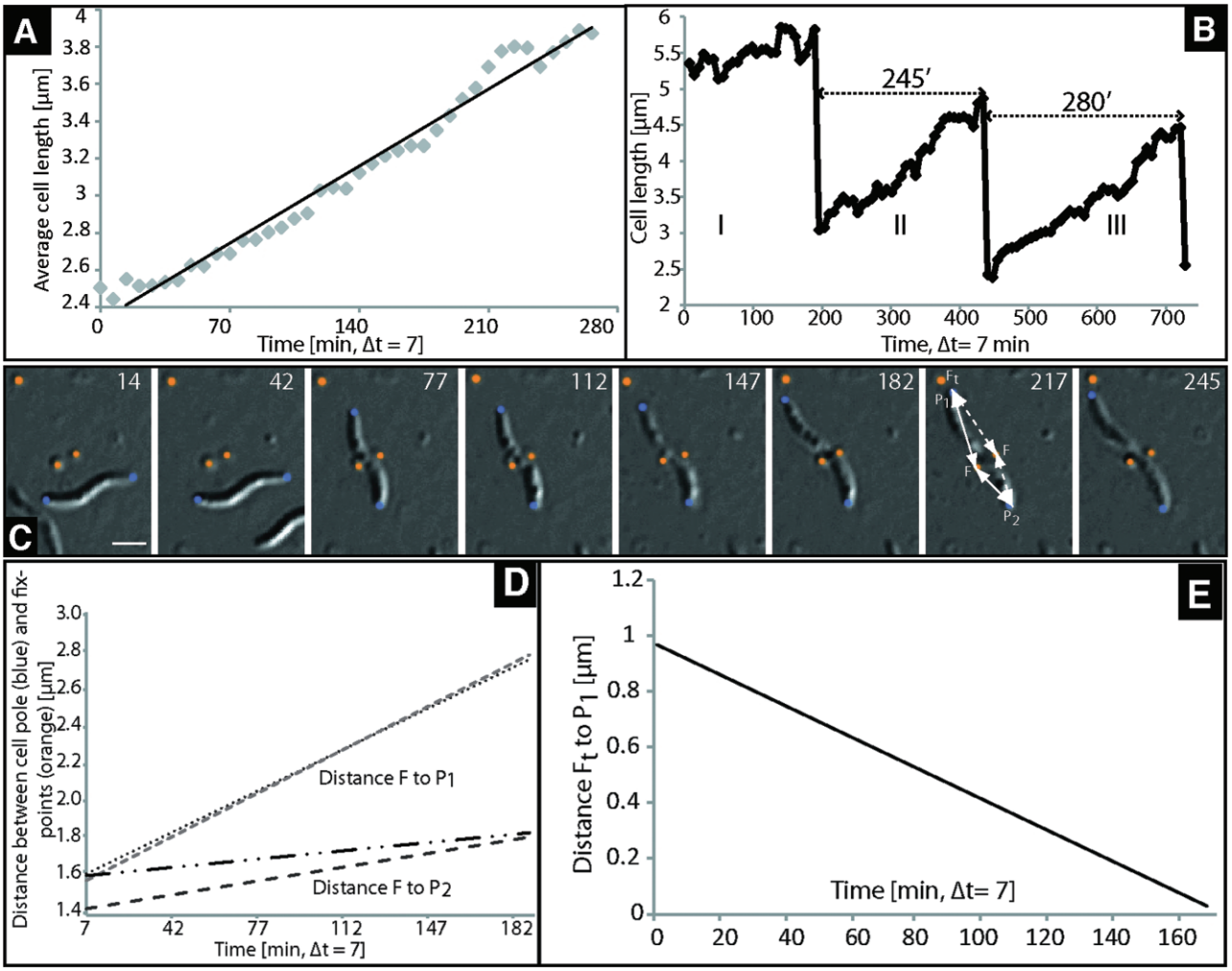

Fig. 2. A. Increase of average cell lengths estimated from time-lapse microscopy of 12 cells over 280 min (equivalent to one generation).
B. Time-course of lengths of a single cell and their offspring followed over two generations. Generation times varied from 240 up to 280 min for completion of a full cycle and maximum length of the mother cells from 5.8 down to 4.5 µm. Number I, II and III correspond to DIC series in Fig. 1C.
C. Individual frames from DIC series of Fig. 1C followed over 245 min showing uneven elongation of a single cell. Scale bar 1 µm. Orange dots: Fixed external reference points on agar surface. Blue points: cell poles.
D. Plot of distances between both cell poles (blue, P1 and P2) and reference points (orange, F and Ft) at cell centre of cell in C over time.
E. Plot of distances between cell pole P1 and external reference point Ft (orange) for cell in C over time.

response. 16 h after cephalexin addition cells were on average 25.6 µm in length and exhibited up to seven stalled constriction sites, which were spaced by about one typical cell length (3.5–4 µm) and considered to be equivalent to three consecutive generations (Fig. 3A–C). Cryo-TEM of WT cells revealed magnetosomes adjacent to cytoskeletal magnetosome filaments, which traversed through the aseptate stalled constriction sites (Fig. 3D). This was also shown by fluorescence microscopy of cephalexin-treated cells expressing an eGFP-MamK fusion. Fluorescence was confined to a filamentous signal running through the elongated cells, indicating that MamK filaments traverse the division plane but are not split. DAPI staining of the cephalexin-treated cells suggested that non-separated daughter cells contained properly segregated chromosomes (Fig. 3G), which indicates that division and separation of magnetosome chains is independent from chromosome segregation.

Many cephalexin-treated WT cells had one long central chain (~10 µm, up to 224 crystals; Fig. S2), which sometimes extended through neighbouring constriction sites. Frequently, 1–3 additional shorter chains (10–30 crystals) were located away from the oldest (i.e. central) division site, which were spaced by large gaps from the primary chain and coincided with younger constrictions. In contrast, cephalexin-treated cells of Δ*mamK* contained up to 19 highly fragmented short subchains (3–38 particles), which were scattered along filamentous

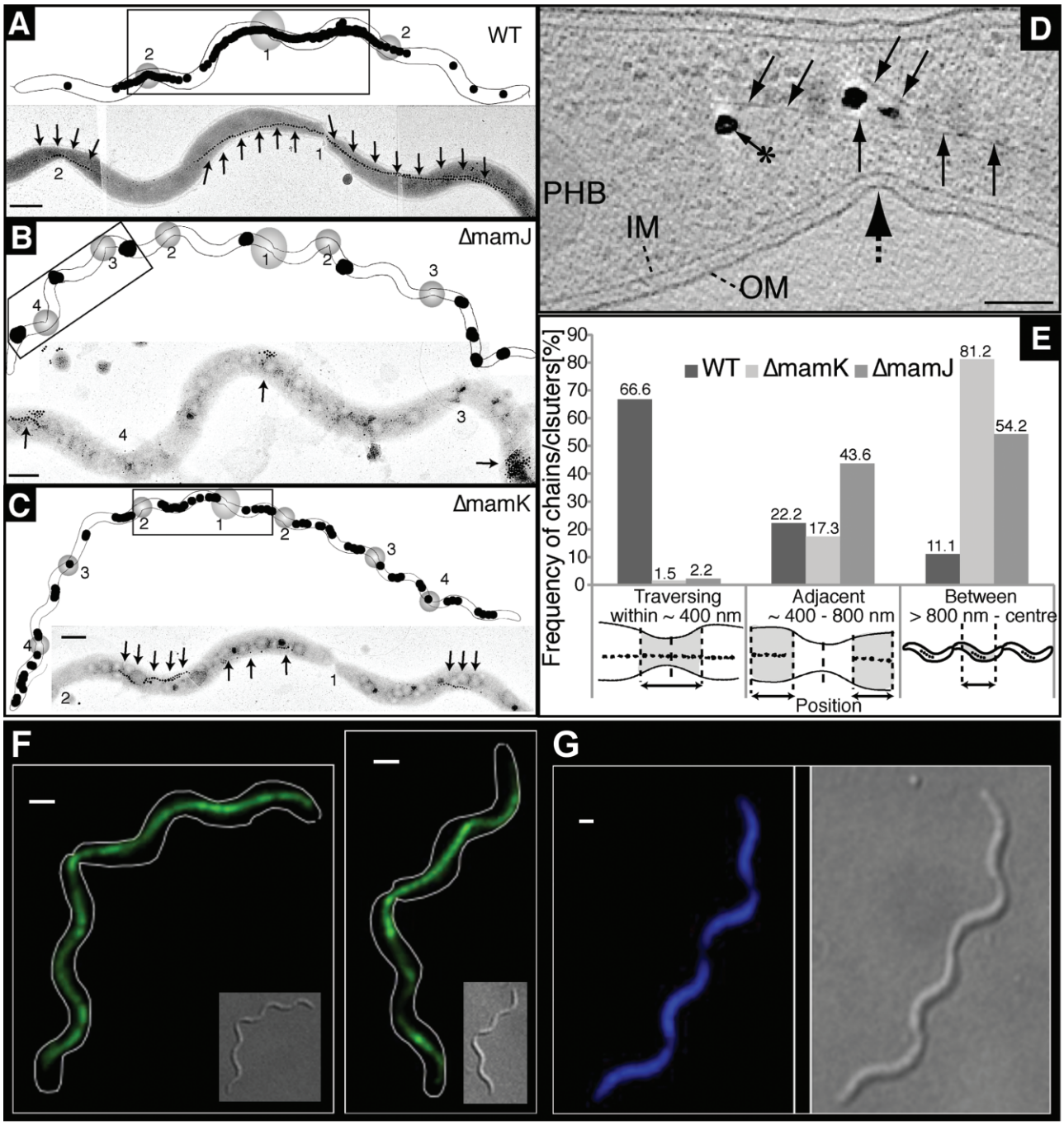

Fig. 3. Cephalexin inhibition in WT, Δ*mamJ* and Δ*mamK*.
A–C. Schematic representations (upper panels) and corresponding TEM micrograph sections (boxes, lower panels) of WT, Δ*mamK* and Δ*mamJ* cells treated with 10 μg ml^{-1} cephalexin for 16 h. Circles: stalled constrictions sites. Big circle: site of first division (oldest). Numbers indicate generations after cephalexin addition. Magnetite particles are highlighted in black (not to scale). Arrows indicate positions of magnetosome chains/clusters. Scale bar 500 nm.
D. Cryo-TEM micrograph of a cephalexin-treated WT cell exhibiting unidirectional constriction (dashed arrow) of the inner and outer membrane (IM, OM). Magnetosome filaments: black arrows, magnetite crystals: arrow with asterisk.
E. Frequency of positions of magnetosome chains or clusters in cephalexin-treated cells of WT, Δ*mamK* and Δ*mamJ*. Magnetosome chain and cluster positions were scored as traversing, adjacent, or between constriction sites as described in the *Experimental procedures* section.
F. Cephalexin-treated WT cells expressing eGFP-MamK (green). Invaginations at midcell indicate blocked septa.
G. DAPI staining of a cephalexin-treated cell. Scale Bars: 1 μm.

cells (Fig. 3C). The positions of chains or clusters were scored in cephalexin-treated cells of WT, Δ*mamK*, and Δ*mamJ* mutants as: (i) traversing (ii) adjacent, or (iii) between the nearest constriction. In the WT most chains were traversing (66.6%), whereas less were adjacent (22.2%) or between (11.1%) constriction sites (Fig. 3E). In Δ*mamK*, only few chains were traversing (1.5%), or adjacent (17.3%), whereas the majority (81.2%) was between constrictions (Fig. 3E). In Δ*mamJ*, only 2.2% of clusters were traversing, whereas similar numbers (43.6% and 54.2%) were either adjacent or between respectively. Comparing those frequencies with their proportions from total cell lengths (traversing: ~10%, adjacent: ~20%, between: ~70%) revealed a strong correlation of magnetosome chain positions with constrictions in the WT, whereas in Δ*mamJ* the clusters were distributed more or less randomly along the cell length. In contrast, there was a negative bias against traversing or adjacent positions of the fragmented chains in Δ*mamK.*

To analyse whether nascent magnetosome chains originated and concatenated from division sites, or alternatively became recruited subsequent to synthesis of particles, we also followed assembly and positioning of chains after induction of magnetite biomineralization in division-inhibited cells. If 50 μM iron citrate was added to iron-starved, cephalexin-inhibited WT cells, magnetosome synthesis could be first detected by magnetic response after about 180 min (Figs 4 and S3). TEM revealed freshly nucleated small crystallites evenly scattered along the entire filament after 180–240 min. After 300 min individual crystals began to concatenate into short precursory chains, resembling the subchains of *Magnetospirillum magneticum*, for which extremely weak magnetostatic interaction fields were estimated (Li *et al.*, 2009). Positions of these precursor chains gradually shifted towards the blocked division sites (Figs 4 and S3). After 480 min, the majority of larger crystals was found in close proximity to constrictions, whereas smaller crystals (< 20 nm) were predominantly localized between them (Figs 4 and S3). Taken together, these results corroborate the notion that magnetosome chains localize dynamically, and indicate that magnetosome chains are recruited to future division sites subsequent to their synthesis by an active mechanism, which is dependent on the presence of MamK.

Magnetosome chain and magnetosome filament are cleaved by asymmetric septation driven by an arc-like Z-ring

Because the unidirectional bending and snapping of cells observed in time-lapse studies and TEM analyses indicated a putative asymmetry in divisome formation and division, structures involved in cellular and magnetosome chain division were further investigated by cryo-electron tomography (CET), which allows three-dimensional reconstruction of cells in an *in vivo* state having preserved all biological structures (Li and Jensen, 2009). About 30 synchronized cells at different stages of division were analysed by CET. We detected a local constriction of the cell envelope at midcell, which progressed down to an annular ring of 250 nm (Fig. 5A). Intriguingly, gradual constriction was followed by unidirectional asymmetric inward growth of the peptidoglycan layer. Even in late stages of division, when the division site was already narrowed to 100 nm, both the magnetosome chain and filament were still intact and ran through the division plane. In 80% of cells, constriction started at a position preferentially opposite to chain and filament, leading to an asymmetric, wedge-like indentation of both structures. After further progression of division, single- or double-stranded magnetosome chains became split and eventually separated by acute bending and asymmetric ingrowth of the septum (Fig. 5Bi–iii). In a very late stage also the cytoskeletal magnetosome filament became bisected (Fig. 5Aiv). Interestingly, flagella already became subterminally inserted in cells before completion of division (Fig. 5Av). Although magnetosome filaments and empty magnetosome membrane vesicles were present in the vicinity of septa, we failed to detect magnetite crystals close to poles immediately after septum closure and separation (Fig. 5Av, Bii), again suggesting that magnetosome chains had rapidly moved away from the poles towards future midcells (Fig. 5Av).

The apparently fixed, preferentially distal localization of the division wedge relative to magnetosome chain and filament raised the question whether the observed asymmetry depends on the presence of chains. We therefore analysed different mutants of MSR deficient in magnetosome synthesis or chain formation. Asymmetric septation and cleavage did not depend on the presence of either MamK (forming the magnetosome filament) or MamJ (connecting magnetosomes to the filament), as isogenic mutants of both genes displayed the same wedge-like septal growth as observed in the WT (Fig. 6). This was also observed in strain MSR-1B in which magnetite crystals, magnetosome membrane vesicles and the magnetosome filament are absent due to deletion of a large part of the magnetosome island (MAI) (Ullrich *et al.*, 2005). This suggests that the wedge-like asymmetric division is independent from the presence of magnetosome chain and filament and must be controlled by determinants encoded elsewhere in the genome.

Careful examination of individual sections from several tomograms of dividing WT cells revealed thin filaments 5–10 nm beneath the cytoplasmic membrane. These short (50–100 nm) filaments extended at constriction sites

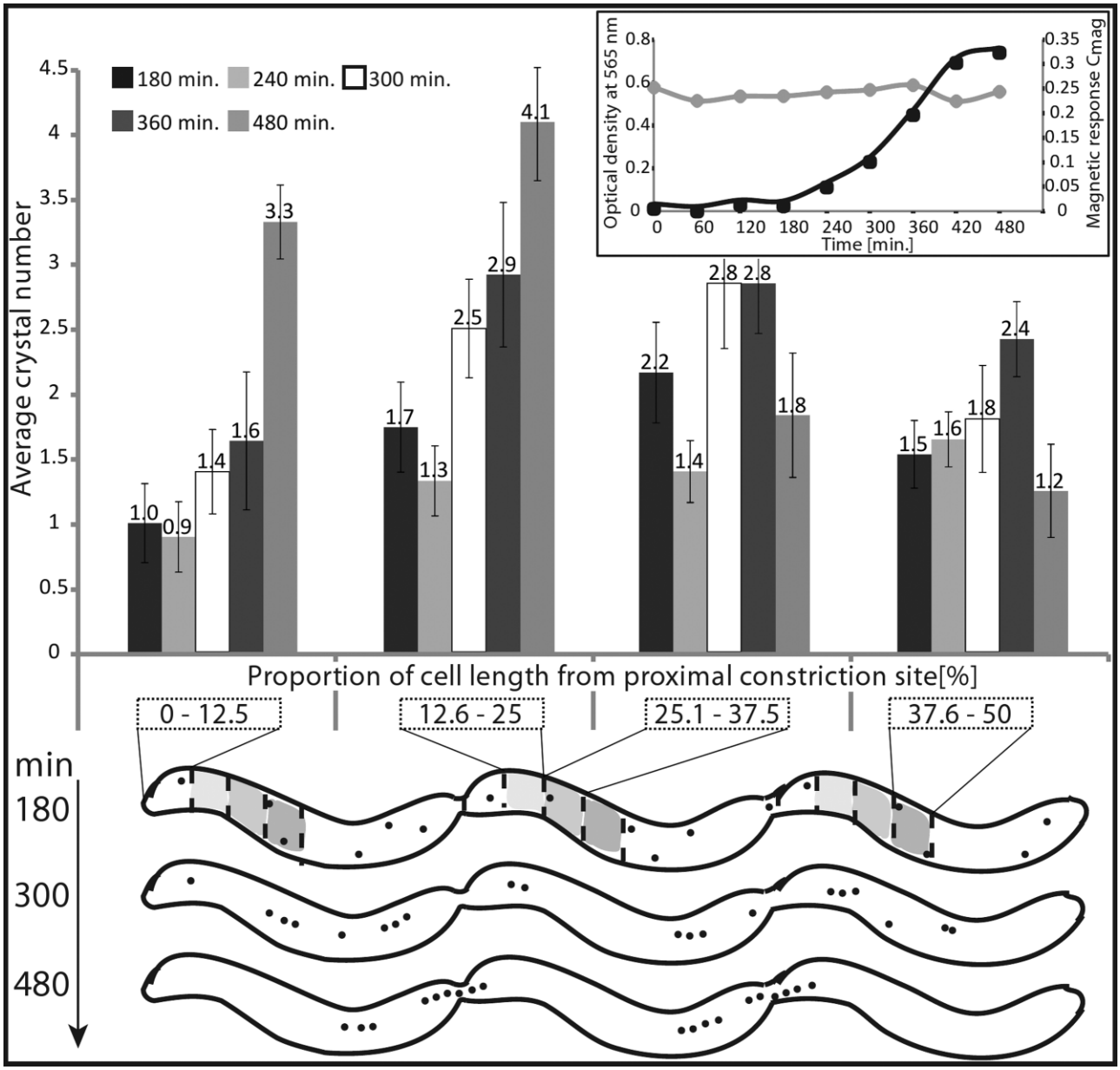

Fig. 4. Dynamic localization of magnetite crystals after induction of magnetite biomineralization in iron-starved, non-magnetic cephalexin-inhibited cells as analysed by TEM. Inset upper right: Growth curve of iron-starved WT cells after 16 h inhibition and subsequent 50 μM iron induction. Optical density (grey) and magnetic response (Cmag, black) are shown. Lower part: Schematic representation of magnetite crystal (black dots) positions within elongated cells at different time points after iron induction and their corresponding relative distances from proximal constriction sites i.e. at relative cell lengths 12.5% from proximal constrictions.

parallel to the division plane. When single images were aligned into a stack, arc-like structures were found adjacent to each other when progressing in z-direction (Fig. 5C and D). The resulting arrangement of the arc-like filaments resembled a tight spiral or pinch as previously observed in *Caulobacter crescentus*, in which arc-like Z-ring structures were predicted (Li *et al.*, 2007). Submembrane localization of the filaments resulted in an 'M'-like overall shape (Fig. 5C and D). Based on these characteristics and its resemblance to the ring described by Li *et al.* (Li *et al.*, 2007), we conclude that this asymmetrical arc-like structure is likely identical with the Z-ring.

Discussion

In this study we present a comprehensive analysis of the cell cycle and cytokinesis in magnetotactic bacteria. Our data suggest that magnetosome chain localization and

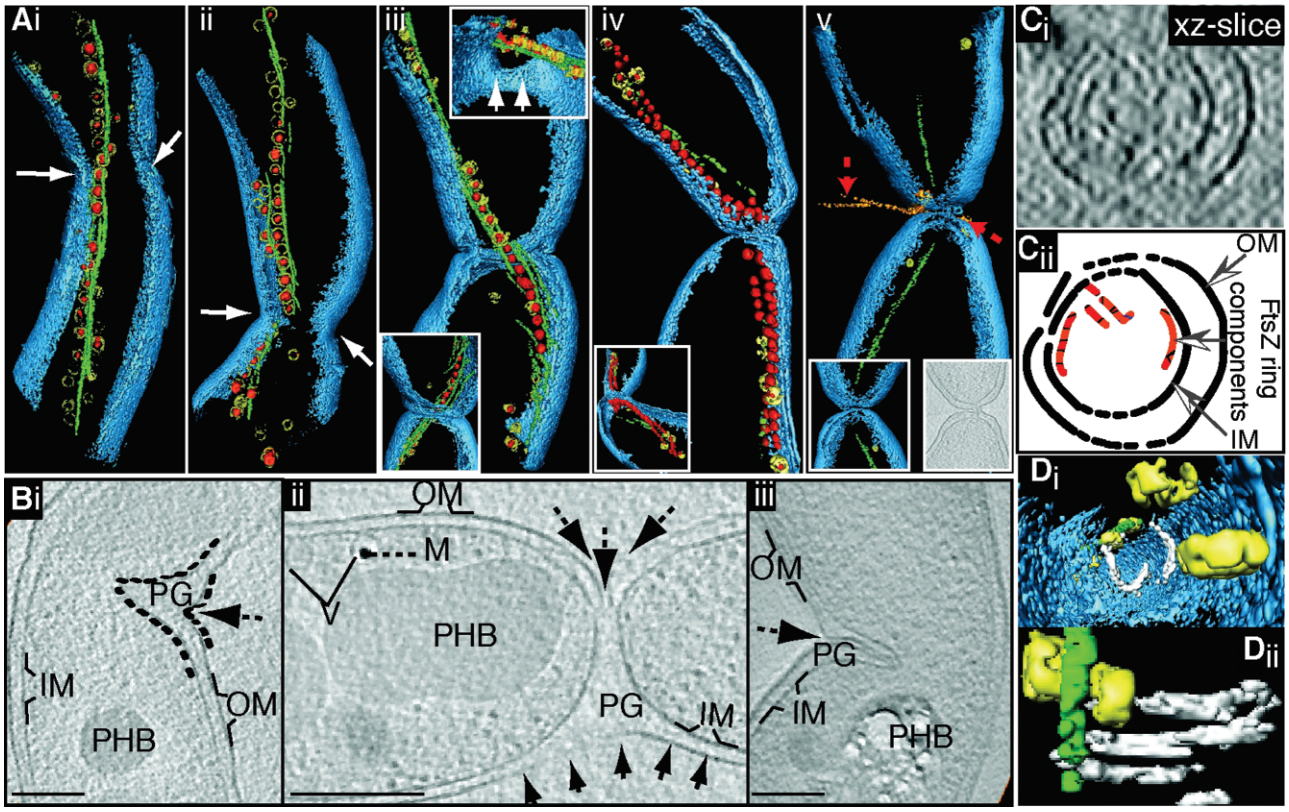

Fig. 5. Segmented tomograms and sections of a tilt series from synchronized MSR cells acquired by CET. Representative tomograms are arranged by progression through cell division.
A. Cell envelope (blue) with constrictions (white arrows). Red: magnetite crystals, yellow: magnetosome membrane and magnetosome filament (green). Insets Aiii–v: different perspective of the tomogram. Inset Av (right): section of tomogram with still connected daughter cells. Orange: flagella (red arrows).
B. Individual sections of tomograms illustrating the asymmetric peptidoglycan (PG) wedge caused by inward growth (dashed arrows) of the outer membrane (OM). Inner membrane (IM), vesicles (V), magnetite crystals (M), and PHB granules are indicated. Scale bar 100 nm.
C. Analysis of Z-ring by CET. i: xz – slice of a WT cell through the constriction site and its schematic segmentation (ii). Dashed line represents the missing wedge, FtsZ ring components in different colours.
D. Tomogram of C segmented at constriction site. Individual Z-arcs (white) show pinch-like localization (ii) just beneath the cell envelope (blue). magnetosome filament: green; magnetosome vesicles: yellow.

segregation is well co-ordinated with cell division by positioning the chains to the future division site subsequent to magnetosome synthesis, which in line with previous speculations (Staniland *et al.*, 2010) is followed by dynamic translocation of chains to midcell after division, carried out according to the scheme in Fig. 7A. In this process, the actin-like MamK protein has a key role as its presence is required for proper magnetosome chain positioning and segregation. The recruitment of chains to stalled constrictions in division-inhibited cells demonstrated that division site recognition is independent from septum formation. So far it remains unknown how division-site positioning is then determined at the molecular level. Apart from the possibility of a geometric cue provided by altered membrane curvature around the constriction site, positional information for division site formation is determined by the Z-ring, preceding the assembly of the multiprotein divisome complex during cytokinesis (den Blaauwen *et al.*, 2008; Goley *et al.*, 2011). It could be envisioned that magnetosome chain localization at midcell might be controlled by early assembling components of the divisomal complex (Fig. 7A), perhaps by direct interaction with the magnetosome filament as it has been speculated based on the discovery of a chimeric protein in which a *mamK* domain is fused to an *ftsZ* domain (Jogler *et al.*, 2009; Katzmann *et al.*, 2010).

After being cleaved at midcell, daughter chains have to be translocated from new cell poles to midcell. The apparent absence of strictly polar magnetosome chain positions in fully separated cells of the WT in our and a previous study (Staniland *et al.*, 2010) suggests that this translocation occurs very fast, i.e. within several minutes or less. Because results of our time-lapse experiments argue against (mono)polar growth, this has to be accomplished by active movement although the molecular mechanism behind this relocalization is not fully clear.

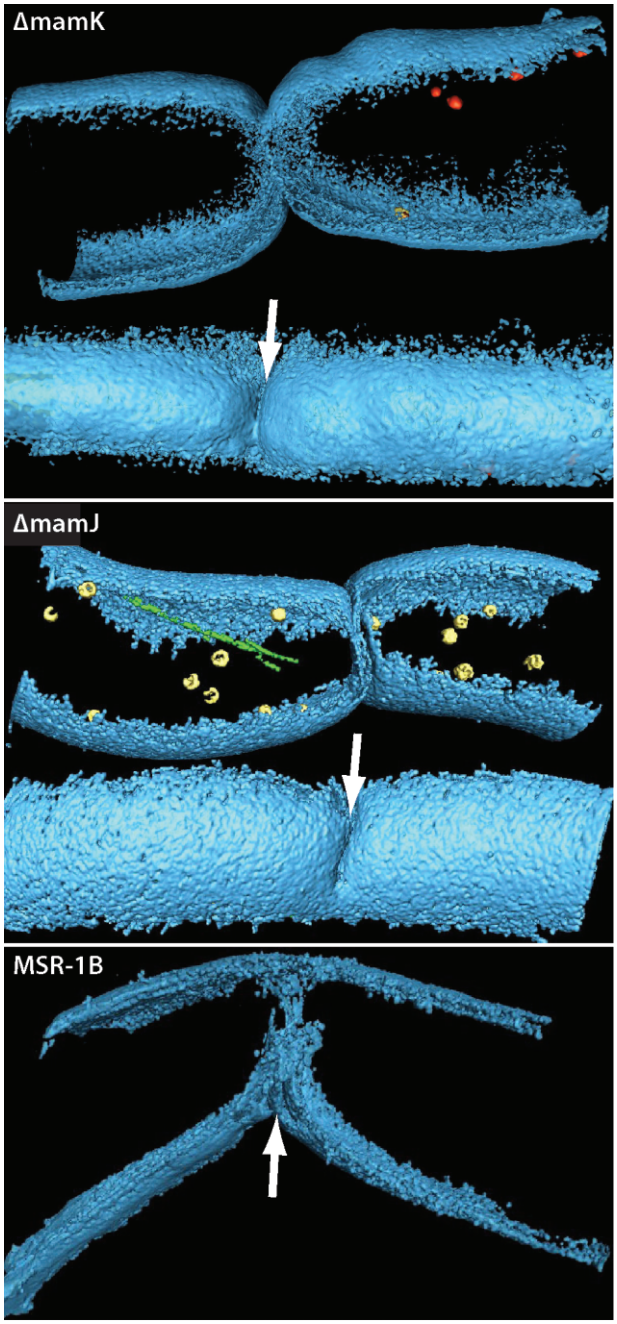

Fig. 6. Segmentations of cryo-electron tomograms of Δ*mamJ*, Δ*mamK* and MSR-1B cells at their constriction sites. White arrows indicate the asymmetric, wedge-ike constriction. Blue: cell envelope, red: magnetite, yellow: magnetosome membrane, green: MamK filament.

There is an increasing number of examples that rapid intracellular movement of organelles, DNA molecules, and protein complexes in bacterial cells is achieved by cytomotive cytoskeletal filaments (Löwe and Amos, 2009; Gerdes *et al*., 2010; Savage *et al*., 2010). For instance, actin-like protein filaments can govern intracellular positioning by providing a track for other proteins to move along (Salje *et al*., 2010). In the related *C. crescentus* disintegration of the polar FtsZ complex is followed by assembly of a Z-ring in proximity of the cell centre, which depends on the activity of the cell division regulator MipZ that is also present in magnetospirilla (Thanbichler and Shapiro, 2006). Assuming a similar mechanism of Z-ring positioning in MSR, we speculate that magnetosome chains may follow the localization of the Z-ring by and along the MamK cytoskeletal filaments (Fig. 7A).

Protein filaments can also lead to force generation by attaching to a structure and actively moving it as a result of filament growth or shrinkage (Salje *et al*., 2010). For example, the *parMRC* system uses bundles of actin-like ParM filaments to push plasmids to opposite poles of the cell, whereupon they are stably inherited on cell division (Salje *et al*., 2010). ParM filaments are dynamically unstable unless bound to plasmids, and thus undergo cycles of growing and shrinking to search the cell space for plasmids. A similar mechanism may well apply to magnetosome chain segregation by the actin-like MamK magnetosome filaments. Instead of pushing, 'treadmilling', i.e. polar depolymerization and shrinkage of MamK filaments anchored at midcell via divisome interaction might generate pulling forces that move magnetosome chains towards future division site (Fig. 6). This mechanism would be also consistent with the results of previous experiments, which revealed that the assembly of MamK filaments expressed in *Escherichia coli* is a highly dynamic and kinetically asymmetrical process and that MamK filaments also displayed intrinsic polarity (Pradel *et al*., 2006). It was also noted in this study that most MamK filaments seemed to be ended at the cellular septa, and it was suggested that short filamentous cables might nucleate at these points and make new filaments in the daughter cells. The assumption that MamK anchored at division sites may actively recruit magnetosome subchains also could explain the abundance of two-stranded chains at constriction sites in the WT, but not in Δ*mamK* (Katzmann *et al*., 2010), because both ends of shrinking MamK filaments could efficiently bind precursor chains synthesized in both of the opposite halves of the predivisional cell, and then concatenate and bidirectionally move them to midcell.

Our time-lapse and electron microscopic analysis revealed that cell division in MSR displays asymmetry along two directions: (i) newborn daughter cells frequently had uneven lengths, and (ii) unidirectional bending, snapping, and septation occurred asymmetrically along the division plane. It has been suggested that length asymmetry might be a feature common to many alphaproteobacteria due to the presence of CtrA regulator, which co-ordinates the cell cycle with asymmetric division in *Caulobacter* (Hallez *et al*., 2004), and is also present in

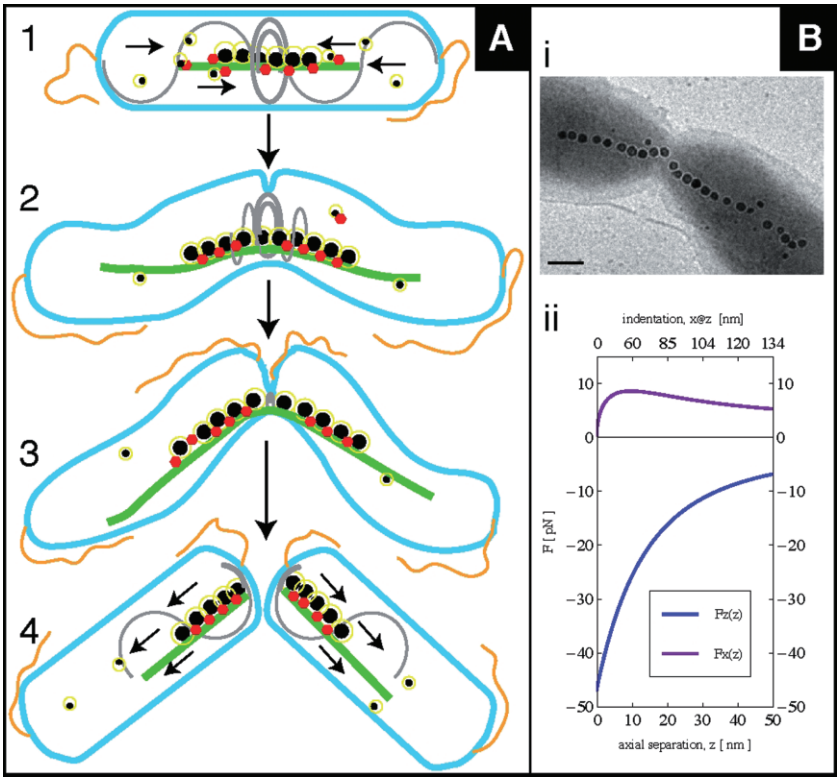

Fig. 7. A. Proposed mechanism of magnetosome chain positioning and division. (1) During cell elongation the magnetosome filament formed by MamK is anchored at midcell to the divisome. By dynamic shrinking of the filament, magnetite crystals bound to the filaments by MamJ, and nascent subchains become concatenated and recruited to midcell. (2) Contraction of the Z arc (grey) results in gradual asymmetric constriction followed by unidirectional inward growth of peptidoglycan. (3) The wedge-like septum causes lateral indentation and acute bending of the magnetosome chain, thereby allowing the adjacent daughter chains to separate against their magnetostatic attraction. Eventually, snapping results in cleavage of the magnetosome chain and filament and breaks the daughter cells apart. (4) Following the divisome to new midcell as determined by the Z arc, split magnetosome chains are rapidly translocated by the magnetosome filament from the new poles of daughter cells towards the future division sites. Blue: cell envelope, green: MamK filament; red: MamJ, black: magnetite crystals, yellow: magnetosome membrane; orange: flagella.
B. Representative TEM image of a dividing MSR cell with lateral indentation of the magnetosome chain (between stage 2 and 3). Scale bar 100 nm. Plots illustrating forces opposing lateral indentation (magenta) and axial separation (blue) during chain division, showing that, owing to its leverage, indentation requires a comparatively small force for magnetosome chain separation.

magnetospirilla (Brilli *et al.*, 2010). However, it requires further clarification if the observed asymmetric division in MSR also reflects functional asymmetry and differentiation as suggested for other Alphaproteobacteria (Hallez *et al.*, 2004).

Cryo-electron tomography analysis indicated a preferred position of the Z-ring and septum distal to the magnetosome chain and the filament. This suggests a controlled mechanism of asymmetric division, which was independent from the presence of magnetosomes, the magnetosome filament, and any genes of the *mamAB*, *mms6* and *mamGFDC* operons of the MAI. Asymmetric constriction and septation might be induced by the arc-shaped Z-ring that we identified by CET. Arc-like FtsZ rings seem to be correlated with asymmetric division in distinct *E. coli ftsZ* mutants (Addinall and Lutkenhaus, 1996) and in cyanelle plastids of some protists, in which the Z-ring extends from one-fourth to one-half way around the cell and is located over a very asymmetrically forming septum (Sato *et al.*, 2007). In MSR, a FtsZ homologue (FtsZm) is encoded within the *mamXY* operon of the MAI (Richter *et al.*, 2007). Although no effect on cell division was reported so far for its deletion in MSR (Ding *et al.*, 2009), it is tempting to speculate that asymmetric ring structures might result from the absence of the binding domain to the membrane tether FtsA in FtsZm. This in turn might cause partial detachment of such a mixed ring from the inner membrane, and consequently, the asymmetric positioning of PG-synthesizing proteins such as FtsI (Fig. 5).

Although bending has been observed in the division of non-magnetic spirilla (Williams, 1959) and magnetic spirilla (Yang *et al.*, 2001; Staniland *et al.*, 2010), asymmetric, wedge-like constriction and septation to our knowledge has not been described before and hence appears to represent a novel and possibly unique mode of

bacterial cell division. This raises the question whether this mechanism reflects a specific adaptation of magnetotactic bacteria in order to split their magnetosome chains. To physically underpin this proposition, we considered the magnetic attraction forces among magnetite crystals in a chain. In MSR, the magnetic attraction is about 40 pN in a one-stranded magnetosome chain (see blue force curve in inset of Fig. 7Bii) and nearly twice as strong in a two-stranded magnetosome chain, but because magnetite crystals in MSR are relatively small and of roughly equidimensional habitus, these figures define rather the lower limit of magnetic attraction forces in a magnetosome chain. Larger crystals of hexagonal prismatic morphology in other magnetotactic bacteria like the magnetic vibrio MV-1 are magnetically held together by attraction forces that well exceed 100 pN (Shcherbakov *et al*., 1997). On top of this, the linear continuity of the cytoskeletal MamK filament to which magnetosomes are attached, must be interrupted too, which requires either additional mechanical forces or cleavage by localized depolymerization (Vats and Rothfield, 2007). We are not aware of a mechanism during cell division that would be capable of producing extensional forces of at least 40 pN acting from the constriction site bidirectionally along the cell axis (Erickson *et al*., 2010). However, through lateral indentation of a magnetosome chain (Fig. 7Bi), the mechanic force required to split the chain could be greatly reduced (from greater than 45 pN to less than 10 pN in the example shown in Fig. 7Bii), owing to leverage. For this mechanism to work, the magnetosome chain must have space to bend away from the indenter. Asymmetric septation is consistent with this geometric requirement.

Recently, it has been demonstrated that intracellular positioning and segregation of bacterial organelles and macromolecular complexes, such as plasmids, chemoreceptors, carboxysomes, and PHB granules (Thompson *et al*., 2006; Galán *et al*., 2010; Savage *et al*., 2010) is governed by dedicated and co-ordinated mechanisms. In conclusion, this study shows that such a mechanism very likely exists also for the highly controlled positioning, division and equipartitioning of bacterial magnetosomes.

Experimental procedures

Bacterial strains, media and growth conditions

Escherichia coli strain DH5α cells (Invitrogen, Karlsruhe, Germany) were used as hosts for cloning. The *dap*$^-$ *E. coli* strain BW29427 was used as donor for transformation of *M. gryphiswaldense* MSR-1 (WT) by conjugation. *E. coli* cultures were grown in lysogeny broth (LB) medium at 37°C shaking supplemented with kanamycin (50 μg ml^{-1}) and 1 mM 2,6-diaminopimelic acid (Sigma-Aldrich, Switzerland) if appropriate. *M. gryphiswaldense* strains were routinely grown microaerobically at 30°C under moderate shaking (120 r.p.m.) in modified FSM medium or in LIM (Low iron media, modified FSM) as described (Heyen and Schüler, 2003; Faivre *et al*., 2007; Lang and Schüler, 2008). For cultivation on solid media, agar was added to 1.5% (wt/vol). Kanamycin was supplied to a final concentration of 5 μg ml^{-1} where necessary. Cephalexin treatment to inhibit cell division was carried out in 1 ml culture volume in 6-well plates under microaerobic conditions. The minimal inhibitory concentration (MIC) of cephalexin for *M. gryphiswaldense* was determined to be 10 μg ml^{-1} by growth experiments with various concentrations of cephalexin accompanied by microscopic inspection of cell morphology, motility and viability (reversibility of the inhibitory effect after removal of the antibiotic). Optical densities and C_{mag} values of MSR cultures were measured turbidimetrically at 565 nm with immotile cells inactivated by the addition of formaldehyde (Fluka, Switzerland) to a final concentration of 0.1% before the measurement. For cell cycle synchronization cells were grown to stationary growth phase in 10 ml FSM hungate vials. Then half of the culture was withdrawn and diluted by fresh modified FSM medium. Cells were grown for 8–12 h at 25°C. The dilution and subsequent growth steps were repeated 4–6 times until > 80% of the cell culture were in division process as verified by light microscopy.

Iron induction experiments

Growth of cephalexin (10 μg ml^{-1}) inhibited cells was performed in microaerobic environment in 24 well plates and 1 ml culture volume over night. For induction of magnetite biomineralization Fe(III)-citrate was supplemented to cells, which were iron starved at aerobic conditions and passaged 4 × in LIM, at a final iron concentration of 50 μM (Scheffel *et al*., 2006; Faivre *et al*., 2007).

Transmission electron microscopy (TEM) and CET

For conventional TEM analysis, unstained cells were absorbed on carbon coated cupper grids (Plano, Wetzlar). Bright field TEM was performed on FEI Tecnai F20 transmission electron microscope (FEI; Eindhoven, The Netherlands) at an accelerating voltage of 200 kV. Images were captured with Eagle 4096 × 4096 pixel CCD camera using EMMenue 4.0 (Tietz, Gauting, Germany) and FEI software. For cryotomography FEI Tecnai F30 Polara transmission electron microscope (FEI; Eindhoven, The Netherlands), equipped with 300 kV field emission gun; Gatan GIF 2002 Post-Column Energy Filters; and 2.048 × 2.048 pixel Multiscan CCD Camera (Gatan; Pleasanton, CA, USA) was used. All data collection was performed at 300 kV, with the energy filter operated in the zero-loss mode (slit width of 20 eV). Tilt series were acquired using Serial EM and FEI software. Quantifoil copper grids (Quantifoil Micro Tools GmbH, Jena) were prepared by placing a 5 μl droplet of 10–15 nm colloidal gold clusters (Sigma) on each grid for subsequent alignment purposes. Additionally a 5 μl droplet of logarithmic MSR-1 culture was added onto the prepared grid, and after blotting embedded in vitreous ice by plunge freezing into liquid ethane (temperature *c.* –170°C). The specimen was tilted typically about one axis with 1.5° increments over a total angular range of +/–65°. To minimize the electron dose

applied to the ice-embedded specimen, data were recorded under low-dose conditions by using automated data acquisition software. The total dose accumulated during the tilt series was kept below 200 e/Å^2. To account for the increased specimen thickness at high tilt angles, the exposure time was multiplied by a factor of 1/cos a. The pixel size in unbinned images was 0.661 at 34 000 magnification, 0.805 at 27 500 magnification and 0.979 at 22 500 magnification. Images were recorded at nominal –8 μm or –4 μm defocus.

CET data analysis

Three-dimensional reconstructions from tilt series were performed with the weighted back-projection method and further analysis of the tomograms was done using the TOM toolbox (Nickell *et al*., 2005). Visualizations of the tomograms were done with Amira (http://www.amira.com) on 2 times binned volumes.

Microscopy and time-lapse experiments

Magnetospirillum gryphiswaldense strains bearing the plasmid pEK42 were grown in 15 ml polypropylene tubes with sealed screw caps and a culture volume of 11 ml to early mid-log phase. A droplet (~ 10 μl) of this culture was fixed to an FSM-agar pad (FSM salts supplemented with 1% agarose) and covered with a coverslip. For staining of nucleic acids, cells were incubated with 10 ng ml^{-1} DAPI for 10 min and immobilized as above. The immobilized cells were imaged with an Olympus BX81 microscope equipped with a 100 × UPLSAPO100XO objective with a numerical aperture of 1.40 and an Orca-ER camera (Hamamatsu). For time-lapse microscopy, cells were fixed on agarose pads and the coverslips with the immobilized cells were placed into a Ludin chamber (Life Imaging Services, Basel, Switzerland) filled with FSM. Cells were imaged with above mentioned microscope and set up. The cell^M autofocus option was set to a range of 5 μm with widths of 1.67 and 0.2 μm for big and small steps respectively. Exposures were recorded every 7 min for 100 cycles and processed using Olympus Xcellence and the GNU Image Manipulation Program (GIMP) software.

Scoring of intracellular magnetosome chain positions

Positions of magnetosome chains in cephalexin-inhibited cells were scored (by the position of the outermost particle of a magnetosome chain/magnetosome cluster nearest to a constriction site) as either (i) traversing: within 400 nm periphery of constrictions (equivalent to the extension of membrane curvature) (ii) adjacent: within ~ 400–800 nm away from nearest constriction (iii) between: more than 800 nm away from the nearest constriction.

Theoretical modelling of forces in a magnetosome chain

Magnetite crystals in magnetosome chains of MSR like those in *M. magnetotacticum* are magnetic single domains (Dunin-Borkowski *et al*., 1998) and have a roughly isometric habitus, which allows us to mathematically describe them as homogenously magnetized spheres, tractable with the dipole formula. Our model magnetosome chain consists of *n* identical magnetosomes, each containing a ferrimagnetic core of diameter *D*, surrounded by a non-magnetic shell of thickness *h* representing the lipid-bilayer membrane of the magnetosome vesicle. Each crystal is magnetized along the chain axis and carries a magnetization equal to the saturation magnetization of magnetite at room temperature (M_s = 470 G). The magnetic dipolar interaction energy of the chain is given by

$$W_n = -\left(\frac{\pi M_s D^3}{6}\right)^2 \sum_{j=1}^{n} \sum_{k=1}^{j-1} \frac{2}{|r_j - r_k|^3}, \quad (1)$$

where r_i and r_j are the position vectors of magnetosomes *j* and *k* respectively. In a close-packed linear chain, we have $|r_j - r_k| = |j - k|(D + 2h)$, where $D + 2h$ is the centre-to-centre distance between any two adjacent particles. Inserting a gap of clear axial distance $z = \gamma(D + 2h)$ between the two innermost magnetosomes (i.e. $j = n/2$ and $k = n/2 + 1$), we obtain the following expression for the magnetostatic interaction energy between two linear magnetosome chain halves separated by a gap *z* along the chain axis:

$$W(z) = -2\left(\frac{\pi M_s}{6}\right)^2 \frac{D^3}{\left(1 + 2h/D\right)^3} \left(\sum_{j=1}^{n/2} \frac{j}{(j+\gamma)^3} + \sum_{j=n/2+1}^{n-1} \frac{(n-j)}{(j+\gamma)^3} \right). \quad (2)$$

The (axial) force F_z holding the two magnetosome chain halves together is easily obtained by taking the derivative of *W(z)*, i.e.

$$F_z(z) = -\frac{dW}{dz} = -\frac{dW}{d\gamma} \cdot \frac{d\gamma}{dz}. \quad (3)$$

$F_z(z)$ is always attractive (negative sign) and is of maximum magnitude at close contact ($z = 0$). For typical magnetosome chain geometries in MSR (D = 42.5 nm, h = 4 nm, n = 10), $F_z(0)$ is about 40 pN. $F_z(z)$ converges quickly with chain length *n*, that is, $F_z(z)$ changes by as little as 2.5% when going from $n = 6$ to $n = 20$. To derive the mechanical force required for magnetosome chain division by lateral indentation (perpendicular to the chain axis), we let the indentation force F_x act on the central part of the magnetosome chain and assume that each chain half is bent into a circular arc, curving away from the indenter while the two (outer) ends of the chain are kept fixed in position (cf. Fig. 7Bi). Then from elementary geometrical considerations, we can express the lateral indentation distance as $x = R(1 - \cos\alpha)$ and the axial separation between the two chain halves as $z = 2R(\alpha - \sin\alpha)$, where $R = (L/2)/\alpha$ is the radius of curvature, $L/2 = (n/2) \cdot (D + 2h)$ is the (arc) length of each magnetosome chain half, and α is the deflection angle (Fig. S4). A relationship between indentation *x* and separation *z* can be obtained by elimination of α, which in first order yields $z \cong 8x^2/(3L)$. This non-linear lever rule *z(x)* can now be used to determine the force required for lateral indentation

$$F_x(z) = \frac{dW}{dx} = \frac{dW}{dz} \cdot \frac{dz}{dx} \cong -4\sqrt{\frac{2\gamma}{3n}} F_z(z), \quad (4)$$

which vanishes at $\gamma = 0$ ($z = 0$), that is, lateral indentation does not require an activation force as opposed to axially

pulling two magnetosome chain halves apart from each other. The maximum of $F_x(z)$ occurs near $\gamma = 1/7$ and is $\sqrt{1/(2n)}$ times smaller in magnitude compared to Fz(0) (cf. Fig. 7Bii).

Acknowledgements

We thank Günter Pfeifer for his continued help with TEM and CET. This research was supported by grants DFG Schu1080/9–1 to D.S. and DFG Wi1828/4–1 to M.W.

References

Addinall, S.G., and Lutkenhaus, J. (1996) FtsZ-spirals and -arcs determine the shape of the invaginating septa in some mutants of *Escherichia coli*. *Mol Microbiol* **22:** 231–237.

den Blaauwen, T., Pedro, M.D., Nguyen-Distèche, M., and Ayala, J.A. (2008) Morphogenesis of rod-shaped sacculi. *FEMS Microbiol Rev* **32:** 321–344.

Brilli, M., Fondi, M., Fani, R., Mengoni, A., Ferri, L., Bazzicalupo, M., and Biondi, E.G. (2010) The diversity and evolution of cell cycle regulation in alpha-proteobacteria: a comparative genomic analysis. *BMC Syst Biol* **4:** 1–16.

Ding, Y., Li, J., Liu, J., Yang, J., Jiang, W., Tian, J., *et al*. (2009) Deletion of the ftsZ-like gene results in the production of superparamagnetic magnetite magnetosomes in *Magnetospirillum gryphiswaldense*. *J Bacteriol* **192:** 1097–1105.

Dunin-Borkowski, R.E., McCartney, M.R., Frankel, R.B., Bazylinski, D.A., Posfai, M., and Buseck, P.R. (1998) Magnetic microstructure of magnetotactic bacteria by electron holography. *Science* **282:** 1868–1870.

Erickson, H., Anderson, D., and Osawa, M. (2010) FtsZ in bacterial cytokinesis: cytoskeleton and force generator all in one. *Microbiol Mol Biol Rev* **74:** 504–528.

Faivre, D., and Schüler, D. (2008) Magnetotactic bacteria and magnetosomes. *Chem Rev* **108:** 4875–4898.

Faivre, D., Böttger, L.H., Matzanke, B.F., and Schüler, D. (2007) Intracellular magnetite biomineralization in bacteria proceeds by a distinct pathway involving membrane-bound ferritin and an iron(II) species. *Angew Chem Int Ed Engl* **46:** 8495–8499.

Faivre, D., Fischer, A., Garcia-Rubio, I., Mastrogiacomo, G., and Gehring, A.U. (2010) Development of cellular magnetic dipoles in magnetotactic bacteria. *Biophys J* **99:** 1268–1273.

Frankel, R., and Bazylinski, D. (2006) How magnetotactic bacteria make magnetosomes queue up. *Trends Microbiol* **14:** 329–331.

Galán, B., Dinjaski, N., Maestro, B., de Eugenio, L., Escapa, I., Sanz, J., *et al*. (2010) Nucleoid-associated PhaF phasin drives intracellular location and segregation of polyhydroxyalkanoate granules in *Pseudomonas putida* KT2442. *Mol Microbiol* **79:** 402–418.

Gerdes, K., Howard, M., and Szardenings, F. (2010) Pushing and pulling in prokaryotic DNA segregation. *Cell* **141:** 927–942.

Goley, E.D., Yeh, Y.-C., Hong, S.-H., Fero, M.J., Abeliuk, E., McAdams, H.H., and Shapiro, L. (2011) Assembly of the *Caulobacter* cell division machine. *Mol Microbiol* **80:** 1680–1698.

Hallez, R., Bellefontaine, A., Letesson, J., and De Bolle, X. (2004) Morphological and functional asymmetry in alpha-proteobacteria. *Trends Microbiol* **12:** 361–365.

Heyen, U., and Schüler, D. (2003) Growth and magnetosome formation by microaerophilic *Magnetospirillum* strains in an oxygen-controlled fermentor. *Appl Microbiol Biotechnol* **61:** 536–544.

Jogler, C., and Schüler, D. (2009) Genomics, genetics, and cell biology of magnetosome formation. *Annu Rev Microbiol* **63:** 501–521.

Jogler, C., Lin, W., Meyerdierks, A., Kube, M., Katzmann, E., Flies, C., *et al*. (2009) Toward cloning of the magnetotactic metagenome: identification of magnetosome island gene clusters in uncultivated magnetotactic bacteria from different aquatic sediments. *Appl Environ Microbiol* **75:** 3972–3979.

Katzmann, E., Scheffel, A., Gruska, M., Plitzko, J.M., and Schüler, D. (2010) Loss of the actin-like protein MamK has pleiotropic effects on magnetosome formation and chain assembly in *Magnetospirillum gryphiswaldense*. *Mol Microbiol* **77:** 208–224.

Komeili, A., Li, Z., Newman, D., and Jensen, G. (2006) Magnetosomes are cell membrane invaginations organized by the actin-like protein MamK. *Science* **311:** 242–245.

Lang, C., and Schüler, D. (2008) Expression of green fluorescent protein fused to magnetosome proteins in microaerophilic magnetotactic bacteria. *Appl Environ Microbiol* **74:** 4944–4953.

Li, J., Pan, Y., Chen, G., Liu, Q., Tian, L., and Lin, W. (2009) Magnetite magnetosome and fragmental chain formation of *Magnetospirillum magneticum* AMB-1: transmission electron microscopy and magnetic observations. *Geophys J Int* **177:** 33–42.

Li, Z., and Jensen, G.J. (2009) Electron cryotomography: a new view into microbial ultrastructure. *Curr Opin Microbiol* **12:** 1–8.

Li, Z., Trimble, M.J., Brun, Y.V., and Jensen, G.J. (2007) The structure of FtsZ filaments *in vivo* suggests a force-generating role in cell division. *EMBO J* **26:** 4694–4708.

Löwe, J., and Amos, L.A. (2009) Evolution of cytomotive filaments: the cytoskeleton from prokaryotes to eukaryotes. *Int J Biochem Cell Biol* **41:** 323–329.

Margolin, W. (2009) Sculpting the bacterial cell. *Curr Biol* **19:** 812–822.

Murat, D., Byrne, M., and Komeili, A. (2010) Cell Biology of Prokaryotic Organelles. *Cold Spring Harb Perspect Biol* **2:** 1–18.

Nickell, S., Förster, F., Linaroudis, A., Net, W., Beck, F., Hegerl, R., *et al*. (2005) TOM software toolbox: acquisition and analysis for electron tomography. *J Struct Biol* **149:** 227–234.

Pogliano, J., Pogliano, K., Weiss, D.S., Losick, R., and Beckwith, J. (1997) Inactivation of FtsI inhibits constriction of the FtsZ cytokinetic ring and delays the assembly of FtsZ rings at potential division sites. *Proc Natl Acad Sci USA* **94:** 559.

Pradel, N., Santini, C.-L., Bernadac, A., Fukumori, Y., and Wu, L.-F. (2006) Biogenesis of actin-like bacterial cytoskeletal filaments destined for positioning prokaryotic magnetic organelles. *Proc Natl Acad Sci USA* **103:** 17485–17489.

Richter, M., Kube, M., Bazylinski, D.A., Lombardot, T., Glöckner, F.O., Reinhardt, R., and Schüler, D. (2007) Comparative genome analysis of four magnetotactic bacteria reveals a complex set of group-specific genes implicated in magnetosome biomineralization and function. *J Bacteriol* **189:** 4899–4910.

Salje, J., Gayathri, P., and Löwe, J. (2010) The ParMRC system: molecular mechanisms of plasmid segregation by actin-like filaments. *Nat Rev Microbiol* **8:** 683–692.

Sato, M., Nishikawa, T., Kajitani, H., and Kawano, S. (2007) Conserved relationship between FtsZ and peptidoglycan in the cyanelles of *Cyanophora paradoxa* similar to that in bacterial cell division. *Planta* **227:** 177–187.

Sato, R., Miyagi, T., Kamiya, S., Sakaguchi, T., Thornhill, R., and Matsunaga, T. (1995) Synchronous culture of *Magnetospirillum* sp. AMB-1 by repeated cold treatment. *FEMS Microbiol Let* **128:** 15–19.

Savage, D., Afonso, B., Chen, A., and Silver, P.A. (2010) Spatially ordered dynamics of the bacterial carbon fixation machinery. *Science* **327:** 1258–1261.

Scheffel, A., and Schüler, D. (2007) The acidic repetitive domain of the *Magnetospirillum gryphiswaldense* MamJ protein displays hypervariability but is not required for magnetosome chain assembly. *J Bacteriol* **189:** 6437–6446.

Scheffel, A., Gruska, M., Faivre, D., Linaroudis, A., Graumann, P.L., Plitzko, J.M., and Schüler, D. (2006) An acidic protein aligns magnetosomes along a filamentous structure in magnetotactic bacteria. *Nature* **440:** 110–114.

Shcherbakov, V., Winklhofer, M., Hanzlik, M., and Petersen, N. (1997) Elastic stability of chains of magnetosomes in magnetotactic bacteria. *Eur Biophys J* **26:** 319–326.

Staniland, S.S., Moisescu, C., and Benning, L.G. (2010) Cell division in magnetotactic bacteria splits magnetosome chain in half. *J Basic Microbiol* **50:** 392–396.

Thanbichler, M., and Shapiro, L. (2006) MipZ, a spatial regulator coordinating chromosome segregation with cell division in Caulobacter. *Cell* **126:** 147–162.

Thompson, S.R., Wadhams, G.H., and Armitage, J.P. (2006) The positioning of cytoplasmic protein clusters in bacteria. *Proc Natl Acad Sci USA* **103:** 8209–8214.

Ullrich, S., Kube, M., Schübbe, S., Reinhardt, R., and Schüler, D. (2005) A hypervariable 130-kilobase genomic region of *Magnetospirillum gryphiswaldense* comprises a magnetosome island which undergoes frequent rearrangements during stationary growth. *J Bacteriol* **187:** 7176–7184.

Vats, P., and Rothfield, L. (2007) Duplication and segregation of the actin (MreB) cytoskeleton during the prokaryotic cell cycle. *PNAS* **104:** 17795–17800.

Williams, M.A. (1959) Cell elongation and division in *Spirillum anulus*. *J Bacteriol* **78:** 374–377.

Yang, C., Takeyama, H., Tanaka, T., Hasegawa, A., and Matsunaga, T. (2001) Synthesis of bacterial magnetic particles during cell cycle of *Magnetospirillum magneticum* AMB-1. *Appl Biochem Biotechnol* **91–93:** 155–160.

Supporting information

Additional supporting information may be found in the online version of this article.

Please note: Wiley-Blackwell are not responsible for the content or functionality of any supporting materials supplied by the authors. Any queries (other than missing material) should be directed to the corresponding author for the article.